HHS Public Access

Author manuscript

Cell Calcium. Author manuscript; available in PMC 2022 October 03.

Published in final edited form as:

Cell Calcium. 2020 May ; 87: 102163. doi:10.1016/j.ceca.2020.102163.

STIM1-Ca^{2+} signaling in coronary sinus cardiomyocytes contributes to interatrial conduction

Hengtao Zhang,

Victoria Bryson,

Nancy Luo,

Albert Y. Sun,

Paul Rosenberg*

Division of Cardiovascular Medicine, Department of Medicine, Duke University School of Medicine, Box 103031 Med Ctr, Durham, NC, 27710, United States

Abstract

Pacemaker action potentials emerge from the sinoatrial node (SAN) and rapidly propagate through the atria to the AV node via preferential conduction pathways, including one associated with the coronary sinus. However, few distinguishing features of these tracts are known. Identifying specific molecular markers to distinguish among these conduction pathways will have important implications for understanding atrial conduction and atrial arrhythmogenesis. Using a *Stim1* reporter mouse, we discovered stromal interaction molecule 1 (STIM1)-expressing coronary sinus cardiomyocytes (CSC)s in a tract from the SAN to the coronary sinus. Our studies here establish that STIM1 is a molecular marker of CSCs and we propose a role for STIM1-CSCs in interatrial conduction. Deletion of *Stim1* from the CSCs slowed interatrial conduction and increased susceptibility to atrial arrhythmias. Store-operated Ca^{2+} currents (I_{soc}) in response to Ca^{2+} store depletion were markedly reduced in CSCs and their action potentials showed electrical remodeling. Our studies identify STIM1 as a molecular marker for a coronary sinus interatrial conduction pathway. We propose a role for SOCE in Ca^{2+} signaling of CSCs and implicate STIM1 in atrial arrhythmogenesis.

Keywords

STIM1; Store-operated calcium entry; Coronary sinus; Atrial fibrillation; Atrial conduction pathways

*Corresponding author. rosen029@mc.duke.edu (P. Rosenberg).

Declaration of Competing Interest

All authors declare no conflicts of interest.

CRediT authorship contribution statement

Hengtao Zhang: Formal analysis. **Victoria Bryson:** Investigation. **Nancy Luo:** Conceptualization, Writing - original draft. **Albert Y. Sun:** Supervision, Investigation. **Paul Rosenberg:** Writing - original draft.

Appendix A. Supplementary data

Supplementary material related to this article can be found, in the online version, at doi:https://doi.org/10.1016/j.ceca.2020.102163.

1. Introduction

Identifying substrates for atrial arrhythmias remain an important research objective; however, current knowledge of normal atrial conduction is incomplete. Cardiac electrical activity initiates normally within the specialized myocardial cells of the sinoatrial node (SAN), rapidly propagating through both atria to the atrioventricular node (AVN). While no macroscopic specialized tracts within the atrial musculature link the cardiac nodes, impulses exiting the SAN spread to the AVN through preferential routes governed by atrial geometry and have been reported to include specialized cell types [1]. Three historically-described tracts facilitate orderly internodal and interatrial depolarization: 1. A bifurcating pathway branching anteriorly from the superior vena cava down the atrial septum and traversing superiorly across to the left atrium (also known as Bachmann's bundle); 2. A middle internodal pathway coursing posterior to the superior vena cava and descending down the atrial septum; and 3. A posterior-inferior pathway descending through the crista terminalis, the valve of the inferior vena cava, and around the coronary sinus (CS) (also called the CS pathway) [2]. Additionally, by connecting the right and left atrium, the CS musculature also contributes importantly to interatrial electrical connection. Impaired conduction through these pathways has been implicated as a mechanism underlying atrial reentrant tachycardias and atrial fibrillation (AF) [3]. However, at present, no molecular markers can distinguish cardiomyocytes of the CS pathway from the rest of the atrium. Given the emerging role of store-operated Ca^{2+} entry (SOCE) in excitable cells, we investigated the anatomical distribution of stromal interaction molecule 1 (STIM1) and its role in atrial conduction. We observed that STIM1 is enriched in an anatomic distribution coinciding with the CS posterior-inferior pathway and may be implicated in its signaling.

Ca^{2+} signaling control pivotal cell functions in both excitable and nonexcitable cells, and calcium-sensing STIM proteins mediate Ca^{2+} homeostasis between plasma membrane depolarization and internal calcium store depletion [4]. STIM1 is a single pass transmembrane phosphoprotein located in the sarcoplasmic reticulum or endoplasmic reticulum (SR/ER), where its activation by depletion of SR calcium stores triggers store-operated Orai and canonical transient receptor potential (TRPC) channels in the plasma membrane. Mice and humans carrying mutations in *Stim1* exhibit defects that include immunodeficiency and a congenital myopathy [5]. In cardiac tissue, many studies have implicated STIM1 in the Ca^{2+} signaling underlying myocyte contraction, growth, and metabolism [6–10]. More recently, we showed that STIM1 is enriched in the SAN where it contributes to automaticity via regulation of the "Ca^{2+} clock" [11]. Here, we characterized the electrophysiology of STIM1-expressing CS cardiomyocytes and defined the role of the STIM1-CS pathway in atrial conduction. These findings implicate STIM1 as a novel marker for the CS internodal conduction pathway and suggest that store-operated calcium entry (SOCE) may have a broader role in atrial arrhythmias than previously appreciated.

2. Methods

2.1. Animals

STIM1-lacZ mice ($STIM1^{+/gt}$) were generated from gene trapped ES cells and genotyped as previously described [12]. $STIM1^{fl/fl}$ mice (C57BL/6) were generated as previously

described [13]. α-MHC (Cardiac specific)-Cre transgenic mice (α-MHC-Cre) (C57BL/6) were obtained from Jackson Laboratories. To generate cardiac specific knockout of STIM1, αMHC-Cre transgenic mice were bred with founder $STIM1^{fl/fl}$ mouse and the progeny $STIM1^{fl/-}$;α-MHC-$Cre^{+/-}$ were then back-crossed with $STIM1^{fl/fl}$ mice. $STIM1^{gt/gt}$ mice and the cardiac restricted mice ($cSTIM1^{-/-}$) were used for cellular studies, as indicated. STIM1 KO mice used for in vivo experiments included the $cSTIM1^{-/-}$ mice for physiologic studies whereas $STIM1^{+/gt}$ mice were used for histological sections. All mice were maintained in pathogen-free barrier facilities at Duke University and were used in accordance with protocols approved by the division of laboratory animal resources and institutional animal care & use committee at Duke University.

2.2. Histochemistry and immunohistochemistry

For whole mount LacZ staining hearts were isolated from mice aged embryonic day 10.5–16 w, dissected and fixed for 20 min. in 2 % PFA PFA with 0.2 % Gluteraldehyde. Tissue was washed in rinse solution (5 mM EGTA, 0.01 % deoxycholate, 0.02 % NP40, 2 mM $MgCl_2$) and stained in LacZ staining solution (5 mM $K_3Fe(CN)_6$, 5 mM $K_4Fe(CN)_6$, 5 mM EGTA, 0.01 % deoxycholate, 0.02 % NP40, 2 mM $MgCl_2$, 1 mg/ml X-gal solution) over night at room temperature. Hearts were then processed for wax sectioning using standard methods and sectioned at 8um. Sections were counterstained using Eosin.

For double labelling with LacZ and antibody staining hearts were snap frozen in OCT and cryosectioned at 14um. LacZ staining was performed on slides as above after fixation for 10 min at room temperature with 4 % PFA. For antibody staining sections were washed PBS, blocked in normal goat serum and stained overnight in primary antibody at 4 °C. After washing and staining with secondary antibody slides were mounted in vectashield. Primary antibodies were as follows Myosin (MF20-DSHB, Iowa), STIM1 (Proteintech Group Inc, IL), HCN4 (Abcam, MA) and SMAA (C6198- Sigma Alderich).

2.3. Coronary sinus cell isolation

Coronary sinus (CS) was identified as the portion of great cardiac vein that begins at the insertion of the oblique vein of Marshall and ends at its orifice in the right atrium. The CS was dissected out and its surrounding tissues including left ventricle and mitral valve were cut off. The CS was cut into several small pieces in prewarmed and oxygenated Tyrode solution containing (in mM): NaCl 140, KCl 5.4, $MgCl_2$ 1.05, NaH_2PO4 0.33, $CaCl_2$ 1.8, HEPES 5, Glucose 10 and pH 7.4. The CS was then incubated in Ca–free solution containing (in mM): NaCl 140, KCl 5.4, $MgSO_4$ 2, NaH_2PO_4 0.33, HEPES 5, Glucose 10, Taurine 5 and pH 7.2, for 10 min at room temperature. The enzymatic digestion solution was prepared with Ca^{2+}-free solution that contains BSA 0.20 %, Collagenase (Type II, Worthington) 0.25 mg/ml. The digestion was monitored every 5 min and was carried out in a shaking incubator at 37 °C. The single cells were released in modified KB solution by gentle titration with a glass transfer pipette. KB Solution includes: KCl 85, K Glutamate 20, KH_2PO_4 20, Taurine 20, EGTA 0.5, Glucose 20, Creatine 5, Succinic Acid 5, Pyruvic Acid 5, $MgSO_4$ 5, HEPES 5, pH 7.2. The isolated CS cells were stored in KB solution at 4 °C at least for 2 h to recover. Those cells having spindle shape with clear striation were chosen for patch clamp experiments.

2.4. Electrophysiology and Ca^{2+} imaging

2.4.1. Fura-2 Ca^{2+} imaging—The isolated coronary sinus myocytes were plated in the 35 mm MatTek glass bottom dish. Fura-2 AM (1 μM) indicator was loaded in normal Tyrode solution at room temperature for 25 min. Fura-2 ratiometric imaging (emission for 340 and 380 nm) then was recorded and analyzed with Metflour software (Molecular device). SR Ca^{2+} store was depleted with a Ca^{2+} free Tyrode solution with a cocktail Ca^{2+} depleting agents containing 30 μM CPA, 10 mM caffeine and 10 μM verapamil. SOCE was measured after SR Ca^{2+} depletion and re-introduction of 2 mM Ca^{2+} Tyrode solution. SOCE was calculated by the initial slope of Ca^{2+} re-entry. All experiments were done at room temperature.

2.4.2. Electrophysiology of CSC myocytes—The isolated single CS cells were placed in a Warner perfusion chamber. The cells were continuously perfused with normal Tyrode solution at a rate of 2 ml/min. The patch pipette was pulled from borosilicate glass capillaries (WPI inc.) with a Sutter P-87 micropipette puller. The pipette usually had a resistance of 3–4 MΩ when filled with pipette solution containing (in mM): NaCl 5, Aspartate acid 140, CsOH, 140, Mg·ATP 2, HEPES 10, BAPTA-K4 10, and pH 7.2. The liquid junction potential was nulled before gigiseal formation. Whole-cell currents were recorded using an AXON AXOPatch 1D amplifier connected to DIGIDATA 1320A digital converter. The currents were activated by a ramp voltage protocol in the range of −110 to +110 mV from holding potential of −40 mV. The currents were filtered at 2 KHz and sampled at a rate of 10 kHz. The data were collected through Clampex software 10.0 (Mol Device) and stored in computer hard drive for further analysis. All experiments were carried out at room temperature.

2.5. Measurement of interatrial conduction time

Activation sequence of electrical activity from SAN to left atrial appendage was determined by simultaneously recordings of surface potentials at left atria and action potentials by means of standard microelectrode technique. A mouse heart was excised and was quickly immersed into pre-warmed and oxygenated Tyrode solution. The ventricles were cut off and atria were open through right atrium to super vena cava (SVC). The CS was open from coronary sinus ostium at right atrium. Bachmann's bundle was incised. Atrial septum and atrioventricular node were also cut off. SAN, left and right atrial appendages were retained. Therefore, electrical pulses generated at SAN were delivered to left atria through coronary sinus. The dissected atria were pinched down with endocardium up to a Warner perfusion chamber and were continuously perfused with Ringer solution bubbling with 95 % O_2 and 5 % CO_2. The chamber temperature was maintained at 30 °C by warner autonomic temperature controller. At this temperature, heart rate was usually near 250 BPM. A patch pipette filled with Ringer solution was used as a surface electrode to record extracellular potentials of left atria. The electrode was placed at the mouth of left atrial appendage and was barely touched with left atria. A traditional microelectrode connected to a Warner intracellular Electrometer (IE-251A) was used to record action potentials. The microelectrode usually had a resistance of 20–60 MΩ and was filled with 2.7 M KCl and 0.3 M K citrate. The conduction time was count as the time from primary sinoatrial node area to left atria.

2.6. ECG and intracardiac electrophysiology studies

Invasive mouse electrophysiology studies were performed as previously described [11]. In brief, mice were anesthetized using 250 mg/kg avertin following institutional guidelines. Anesthetized mice were placed on a heating pad (37 °C) for temperature control. Surface ECG recordings were obtained with subcutaneously placed 29-gauge needle electrodes connected to a ML138 Octal Bioamp (ADInstruments Colorado Springs, CO) and a Powerlab 16/30 acquisition system (ADInstruments) in both forelimbs and hindlimbs to create a Lead I and Lead II configuration. A cutdown of the internal jugular vein was performed, and an EPR-800 1.1 F octapolar catheter (Millar Instruments, Houston, TX) was advanced into the right atrium, atrioventricular junction and right ventricle under intracardiac electrogram guidance. Programmed stimulation was performed at twice diastolic threshold using the Powerlab 16/30 Voltage stimulator (ADInstruments). Surface and intracardiac ECGs were sampled at 2 kHz, filtered between 0.3 Hz and 1 kHz and analyzed with LabChart Pro 7.2 software (ADInstruments). Cardiac cycle intervals (milliseconds) were averaged from 5 consecutive PQRS complexes. Between each stimulation, the mice were allowed to recover for at least 30 s.

2.7. Data analysis

Averaged results are presented as mean ± SEM. Based on a power calculation using a 95 % confidence interval and assuming a 20 % difference in the magnitude of the effect between groups, a sample size of n (mice, SAN tissue or cells) for each group was between 8–20 to achieve a statistical power of 80 % (beta = 20 %). Mice (WT v KO) were allocated randomly for ECG recording, in vivo electrophysiology, and imaging, otherwise no randomization was performed. The principal operator was blinded to the genotypes for in vivo procedures. Comparisons were made among gender and age-matched controls for several independent litters. No data was excluded from analysis except that obtained from mice that died periprocedurely. All data points represent biologic replicates. Population means were tested for significance using a student two-tailed *t*-test P value < 0.05 was considered significant.

3. Results

3.1. STIM1 Expression in Mouse Coronary sinus identifies a unique interatrial conduction pathway

To define STIM1 expression in the heart, we exploited the β-galactosidase reporter from *Stim1* gene trap mice (STIM1-LacZ) [12]. STIM1-LacZ was detected in the SAN, at the junction between the superior vena cava and the right atrial appendage, as we recently demonstrated [11]. From whole mount images of the whole heart or atria, the STIM1-LacZ staining was found to extend from the inferior vena cava to the SAN. We also detected staining in the coronary sinus (Fig. 1A and E). The STIM1-LacZ was present in a well-demarcated, continuous pattern, as evident on serial sections, from the SAN to the coronary sinus (supplemental Fig. 1). Tracing the expression of STIM1-LacZ from the SAN posteriorly into the LA raised the possibility that STIM1 demarcated a specific tract connecting the SA node and the coronary sinus in the posterior-inferior pathway (Fig. 1B–D, F–G and supplemental Fig. 1). This STIM1-positive tract ended just above the AVN in the neonatal P10 heart which was apparent from labelling with HCN4, a well-established

marker of the AVN in neonatal hearts (Fig. 1H,I) [14]. During development, STIM1 was expressed early and in regions that contribute to the future SAN and CS. Supplemental Fig. 2 shows that STIM1 was detected in the embryonic sinus venosus (e12.5), which is known to contribute cells to the SAN and coronary sinus. We have been unable to identify a molecular marker with an expression pattern similar to that demonstrated for STIM1. STIM1-LacZ was also detected in the aorta and pulmonary veins to a lesser extent, but the STIM1-LacZ in the great vessels was discontinuous and distinct from the staining in the SAN-CS (Supplemental Fig. 1). We therefore suggest this may represent the first marker for an atrial conduction pathway.

3.2. STIM1 resides in coronary sinus cardiomyocytes

We next sought to define the cell type expressing STIM1 in this atrial conduction pathway. Using cryosections from atria of 16-week old WT mice, we co-labeled STIM1 with cardiac muscle markers (MF20) that identify cardiac myosins. We detected STIM1 in a subset of MF20+ cells that are present near the coronary sinus (Fig. 2A). This pattern of STIM1 expression in the coronary sinus corresponds to that of the STIM1-LacZ detected above sections (Fig. 1 H–I, Supplemental Fig. 3B). In contrast, immunostaining with smooth muscle α-actin antibody in the atrial cryosection exhibited a pattern distinct from STIM1-LacZ staining (Supplemental Fig. 3A). Based on these studies, a subset coronary sinus cardiomyocytes (CSC) can be defined by the presence of STIM1 while surrounding atrial cardiomyocytes lack STIM1.

3.3. SOCE is enhanced in coronary sinus cardiomyocytes and requires STIM1

CSC loaded with Fura-2 were subjected to a store depletion-Ca^{2+} readdition protocol to evaluate SOCE. External solutions were switched to 0 Ca^{2+} with CPA to block refilling of stores by SERCA2a and with caffeine to release RYR2 Ca^{2+} stores. SOCE is evaluated upon readdition of 2 mM Ca^{2+} in the presence of CPA (Fig. 2B, left). WT CSCs exhibit clear differences in the magnitude of SOCE: 58 % of CSC exhibited moderate SOCE as assessed by the slope of SOCE (0.01–0.001), 15 % exhibited large SOCE (> 0.01), or 30 % of CSC with small SOCE (< 0.001) (Fig. 2B, right). These data support the view that SOCE is present only in a subset of CS cardiomyocytes (Fig. 2A). We also show that STIM1 is required for activation of SOCE. Compared to WT, CSC isolated from STIM1 KO mice exhibit markedly reduced SOCE. In fact, the rate of SOCE in the WT CSCs that were incubated with La^{3+} (10μM) to block all SOCE was similar to KO CSC (Fig. 2B, 2C). We also detected reduced release of Ca^{2+} from internal stores in the CSC of KO mice compared to WT. Here, CSCs are incubated with no external Ca^{2+} and CPA to block store refilling and caffeine to release RYR2 stores. We show that area under the curve (AUC) for the KO CSC was markedly reduced compared with WT (Fig. 2C, right panel). Notably basal Ca^{2+} was not different in these experiments (Fig. 2C, left panel).

3.4. STIM1 regulates a store-operated Ca^{2+} current in coronary sinus cardiomyocytes

Because STIM1 is known to activate SOC current (I_{soc}) in response to Ca^{2+} store depletion in many cell types, we designed experiments to determine whether STIM1 functioned in a similar role in CSCs using whole cell patch clamp technique. I_{soc} was measured from CSCs isolated from WT and STIM1 KO mice. Ca^{2+} stores were depleted to activate I_{soc} currents

by the inclusion of the Ca^{2+} chelator BAPTA (10 mM) to the internal pipette solutions. Resting membrane potentials were held at −80 mV to mimic physiologic conditions, and Ba^{2+} was used as the charge carrier and to eliminate contaminating currents from K^+ channels as is apparent after switching from Tyrode's solution to recording solutions. With this approach, I_{soc} was present in WT CSCs but was markedly reduced in STIM1 KO CSCs. For comparison, we also provided I_{soc} recordings from atrial cardiomyocytes from WT mice (Fig. 3A). The persistence of the current in the WT CSCs is consistent with a Ba^{2+} current that was not present in the STIM1 KO CSCs or WT atrial cardiomyocytes. We interpret these findings as evidence for a Ba^{2+} current found specifically in CSCs that responds to store depletion and requires STIM1 for activation. To gather additional details about this current, a ramp protocol was then used to construct current-voltage relationships for WT and STIM1 KO CSCs after store depletion (Fig. 3B). Specific features of the I_{soc} recorded in CSCs included a linear current voltage (I–V) relationship with a 0 mV reversal potential (Fig. 3C). Confirming that this current was I_{soc}, it was readily inhibited by the addition of Gd^{3+} (20 μM), a known SOC channel inhibitor (Fig. 3A, 3D). These results provide clear evidence that STIM1 participates in I_{soc} in CSCs.

3.5. STIM1-currents and the action potential of CSCs

To understand whether the STIM1 activated currents influenced the resting membrane potential and thus the action potential, we measured AP in freshly isolated CS tissue. Action potentials recorded from CSCs from STIM1 KO mice revealed a more depolarized resting membrane potential (RMP) than those recorded from CSCs recorded from WT mice (Fig. 4D and Table 1). As a consequence of depolarized RMP, the upstroke rate of action potentials was slower in the STIM1 KO CSCs (Fig. 4D). The AP duration at 90 % (APA90) recorded from CSCs lacking STIM1 was also significantly prolonged compared to WT CSCs. It is apparent from these results that deletion of STIM1 and the inward SOC current activated by STIM1 from the CSCs resulted in significant remodeling of the action potential of individual CSCs. Whether these alterations in the electrophysiological properties of the CMCs would influence the AP propagation throughout the atria was tested next.

3.6. Deletion of STIM1 from coronary sinus impair atrial conduction

To determine if STIM1-postitive CMCs contribute to atrial conduction, we mapped electrical pulse generation in the SAN and impulse propagation to the left atrium through the CS pathway using an *ex vivo* preparation prepared from hearts isolated from STIM1 WT and KO mice. Atria including the SVC-SAN were dissected from WT and KO hearts. Atria were open through an incision that bisects the right atria and SVC. Atrial septum and Bachmann bundle were incised in order to block conduction through these alternative pathways (Fig. 4A, blue dash lines). A reference electrode (RE) was placed in the left atrium and recording electrodes (Fig. 4B as indicated by the lower case letters a–f) were placed in the regions spanning the SA node, crista terminalis, inferior vena cava, and coronary sinus. Using the conduction maps generated from these studies, we calculated the conduction times through this pathway (ΔT/√CL, normalized to cycle length). Conduction through the atria of STIM1 KO mice was significantly prolonged compared to WT littermates (1.5 ± versus 0.5 ± ms of ΔT/√CS, Fig. 4C). Taken together, these studies show selective deletion of STIM1

from cardiomyocytes slowed impulse propagation from the SAN to the LA only through a specific atrial pathway involving the CS.

3.7. Conduction abnormalities in cSTIM1$^{-/-}$ mice in vivo

We next sought evidence for the functional consequence of the STIM1 pathway in the murine hearts using surface electrocardiography (ECG). In anesthetized cSTIM1$^{-/-}$ and WT mice, we first examined the P wave duration—an indicator of atrial depolarization—and the PR interval—a marker of conduction time between SA and AV nodes—on surface ECG recordings (Lead I and II). These data imply that interatrial conduction is normal in the cSTIM1$^{-/-}$ hearts and thereby reflects functional interaction of the three internodal conduction pathways. Cholinergic stimulation was then used to draw out the conduction abnormalities *in vivo* by slowing conduction in CMs. Following intraperitoneal injection of carbachol (CCh, 100 ng/g), the PR internal of cSTIM1$^{-/-}$ mice was significantly longer than WT mice (Fig. 5C). Moreover, the P-wave morphology was biphasic and wider in cSTIM1$^{-/-}$ mice supporting delayed internodal conduction (Fig. 5A and B).

3.7.1. cSTIM1$^{-/-}$ mice are vulnerable to atrial arrhythmias—We next tested the hypothesis that delayed conduction through the CS pathway would predispose hearts to arrhythmias including atrial fibrillation. Catheters placed in the right atrium were used for invasive programmed stimulation. WT and cSTIM1$^{-/-}$ mice were subjected to rapid atrial pacing as a method to assess susceptibility to atrial fibrillation. The cSTIM1$^{-/-}$ mice were easily stimulated into atrial fibrillation characterized by a rapid and irregular cycle lengths (Fig. 5D, 9/10 hearts). In contrast, burst pacing triggered atrial fibrillation in hearts of STIM1$^{fl/fl}$ mice only rarely (1/10 hearts) indicating a significant increase in the induction of atrial fibrillation in the cSTIM1$^{-/-}$ mice ($p < 0.001$). In cSTIM1$^{-/-}$ mice, changes in the electrophysiological properties of the CMCs may have increased susceptibility to atrial fibrillation. We also noted in the cSTIM1$^{-/-}$ mice that the duration of AF was prolonged indicating that the rhythm was stable. When STIM1 is deleted in the SAN and internodal CS pathway, our results suggest delayed interatrial conduction may be implicated in the formation of reentrant circuits and atrial tachyarrhythmias.

4. Discussion

Accelerated conduction from the SAN to AVN has long been proposed to occur via preferential pathways that contribute to atria depolarization, but at present, no molecular markers can distinguish cardiomyocytes of these pathways from the rest of the atrium. Here, we report for the first time a role for STIM1 as a marker of CSCs in the posterior-inferior conduction pathway of the mouse atrium. Our anatomical studies show that STIM1 expression in the adult mouse heart was preferential to the cardiomyocytes of the SAN and those cardiomyocytes ensheathing the coronary sinus (CSCs). Our electrophysiological studies show that CSCs lacking STIM1 undergo extensive electrical remodeling that predisposes cSTIM1$^{-/-}$ mice to delayed impulse conduction and atrial arrhythmias. Taken together these data suggest that STIM1 defines a novel pathway in the mouse heart that is involved in the propagation of electrical impulses through the posterior-inferior internodal conduction pathway.

4.1. STIM1 activates a non-selective SOC current in cardiomyocytes

As a Ca^{2+} sensor, STIM1 activates both known types of SOCE channels identified, Orai and TRPC. In SANCs, which we showed selectively express Orai1 channels, we recently postulated that the SOC current (I_{soc}) activated by STIM1 is mediated through Orai1 [6,10,11]. With high Ca^{2+} selectivity and inward rectification, the I_{soc} from SANC strongly resemble currents from Orai1. Here, however, we noted an important distinction between I_{soc} from CSCs and those recorded from SANCs. In CSCs, I_{soc} exhibited a linear current-voltage relationship with a 0 mV reversal potential, suggesting a current of non-selective cation channels permeable to both Na^{+} and Ca^{2+} and therefore highly resembling a TRP channel. It is likely that ventricular, CSCs and SAN cardiomyocytes express different SOC channels [11]. While Orai1 channels have not been found in ventricular cardiomyocytes [6,10], several TRP channels are expressed in atrial and ventricular cardiomyocytes [15–19]. Therefore, we postulate that in CSCs, STIM1-dependent I_{soc} involves activation of TRPC channels.

4.2. STIM1-Ca2+ signaling is important for interatrial conduction

We observed extensive electrical remodeling in $STIM1^{-/-}$ CSCs and showed that these changes could alter arrhythmia susceptibility. Under cholinergic stimulation—which lowers the resting membrane potential and slows overall conduction, $cSTIM1^{-/-}$ CSCs exhibited greater electrical distortion in internodal conduction as exhibited by surface electrocardiography and with program stimulation, much greater susceptibility for initiation of atrial fibrillation. CSCs are a known source for reentrant circuits and atrial tachyarrhythmias [20–22]. Additionally, TRP channels have also been implicated in the arrhythmogenesis and maintenance of atrial fibrillation [23,24]. Taken together, our findings support the importance of STIM1 signaling in the unique CS conduction pathway and the development of clinical atrial arrhythmias.

4.3. STIM1 defines a novel conduction pathway in the mouse heart

Results of our studies provide the first evidence for a molecular marker of the posterior-inferior internodal atrial conduction pathway. STIM1 distribution during cardiac development and in the adult heart is consistent with a specific inferior-posterior pathway. Several studies has suggested that STIM1 is present in cardiomyocytes of the mouse heart and contributes to Ca^{2+} store refilling. By using STIM1 reporter mice, we identified the specific cardiac myocytes and characterized the function of STIM1-Ca^{2+} signaling in these cells. Our studies characterize how STIM1 influences electrical remodeling in these specialized cardiomyocytes, providing novel mechanistic insight as to how localized regions like the CS can contribute to the development of atrial arrhythmias. We also established a molecular mechanism underlying the interatrial conduction pathway that connects the SAN, right and left atrium through the coronary sinus. These findings have important implications for STIM1 as a therapeutic target in atrial arrhythmogenesis.

Supplementary Material

Refer to Web version on PubMed Central for supplementary material.

Acknowledgements

This project was supported by Award Number AG045551 (PBR) and DK109911 (PBR). The content is solely the responsibility of the authors and does not necessarily represent the official views of the National Institutes of Health (NIA, NIDDK and NCHID) United States of America. Award Numbers AG045551.

References

[1]. Liebman J, Are there internodal tracts? Yes, Int. J. Cardiol. 7 (1985) 175–185. [PubMed: 3882584]

[2]. James TN, The development of ideas concerning the conduction system of the heart, Ulster Med. J. 51 (1982) 81–97. [PubMed: 6761929]

[3]. Schotten U, Verheule S, Kirchhof P, Goette A, Pathophysiological mechanisms of atrial fibrillation: a translational appraisal, Physiol. Rev. 91 (2011) 265–325. [PubMed: 21248168]

[4]. Wang Y, Deng X, Mancarella S, Hendron E, Eguchi S, Soboloff J, Tang XD, Gill DL, The calcium store sensor, STIM1, reciprocally controls Orai and CaV1.2 channels, Science 330 (2010) 105–109. [PubMed: 20929813]

[5]. Feske S, ORAI1 and STIM1 deficiency in human and mice: roles of store-operated Ca2+ entry in the immune system and beyond, Immunol. Rev. 231 (2009) 189–209. [PubMed: 19754898]

[6]. Zhao G, Li T, Brochet DX, Rosenberg PB, Lederer WJ, STIM1 enhances SR Ca2+ content through binding phospholamban in rat ventricular myocytes, Proc Natl Acad Sci U S A 112 (2015) E4792–4801. [PubMed: 26261328]

[7]. Hulot JS, Fauconnier J, Ramanujam D, Chaanine A, Aubart F, Sassi Y, Merkle S, Cazorla O, Ouille A, Dupuis M, Hadri L, Jeong D, Muhlstedt S, Schmitt J, Braun A, Benard L, Saliba Y, Laggerbauer B, Nieswandt B, Lacampagne A, Hajjar RJ, Lompre AM, Engelhardt S, Critical role for stromal interaction molecule 1 in cardiac hypertrophy, Circulation 124 (2011) 796–805. [PubMed: 21810664]

[8]. Collins HE, Zhu-Mauldin X, Marchase RB, Chatham JC, STIM1/Orai1-mediated SOCE: current perspectives and potential roles in cardiac function and pathology, Am. J. Physiol. Heart Circ. Physiol. 305 (2013) H446–458. [PubMed: 23792674]

[9]. Touchberry CD, Elmore CJ, Nguyen TM, Andresen JJ, Zhao X, Orange M, Weisleder N, Brotto M, Claycomb WC, Wacker MJ, Store-operated calcium entry is present in HL-1 cardiomyocytes and contributes to resting calcium, Biochem. Biophys. Res. Commun. 416 (2011) 45–50. [PubMed: 22079292]

[10]. Rosenberg P, Socking it to cardiac hypertrophy: STIM1-mediated Ca2+ entry in the cardiomyocyte, Circulation 124 (2011) 766–768. [PubMed: 21844088]

[11]. Zhang H, Sun AY, Kim JJ, Graham V, Finch EA, Neplioueev I, Zhao G, Li T, Lederer WJ, Stiber JA, Pitt GS, Bursac N, Rosenberg PB, STIM1-Ca2+ signaling modulates automaticity of the mouse sinoatrial node, Proc. Natl. Acad. Sci. U. S. A. 112 (2015) E5618–5627. [PubMed: 26424448]

[12]. Stiber J, Hawkins A, Zhang ZS, Wang S, Burch J, Graham V, Ward CC, Seth M, Finch E, Malouf N, Williams RS, Eu JP, Rosenberg P, STIM1 signalling controls store-operated calcium entry required for development and contractile function in skeletal muscle, Nat. Cell Biol. 10 (2008) 688–697. [PubMed: 18488020]

[13]. Oh-Hora M, Yamashita M, Hogan PG, Sharma S, Lamperti E, Chung W, Prakriya M, Feske S, Rao A, Dual functions for the endoplasmic reticulum calcium sensors STIM1 and STIM2 in T cell activation and tolerance, Nat. Immunol. 9 (2008) 432–443. [PubMed: 18327260]

[14]. Marger L, Mesirca P, Alig J, Torrente A, Dubel S, Engeland B, Kanani S, Fontanaud P, Striessnig J, Shin HS, Isbrandt D, Ehmke H, Nargeot J, Mangoni ME, Functional roles of Ca(v)1.3, Ca(v)3.1 and HCN channels in automaticity of mouse atrioventricular cells: insights into the atrioventricular pacemaker mechanism, Channels Austin (Austin) 5 (2011) 251–261.

[15]. Xie J, Cha SK, An SW, Kuro OM, Birnbaumer L, Huang CL, Cardioprotection by Klotho through downregulation of TRPC6 channels in the mouse heart, Nat. Commun. 3 (2012) 1238. [PubMed: 23212367]

[16]. Seth M, Zhang ZS, Mao L, Graham V, Burch J, Stiber J, Tsiokas L, Winn M, Abramowitz J, Rockman HA, Birnbaumer L, Rosenberg P, TRPC1 channels are critical for hypertrophic signaling in the heart, Circ. Res. 105 (2009) 1023–1030. [PubMed: 19797170]

[17]. Ohba T, Watanabe H, Murakami M, Sato T, Ono K, Ito H, Essential role of STIM1 in the development of cardiomyocyte hypertrophy, Biochem. Biophys. Res. Commun. 389 (2009) 172–176. [PubMed: 19715666]

[18]. Nakayama H, Wilkin BJ, Bodi I, Molkentin JD, Calcineurin-dependent cardiomyopathy is activated by TRPC in the adult mouse heart, FASEB J. 20 (2006) 1660–1670. [PubMed: 16873889]

[19]. Onohara N, Nishida M, Inoue R, Kobayashi H, Sumimoto H, Sato Y, Mori Y, Nagao T, Kurose H, TRPC3 and TRPC6 are essential for angiotensin II-induced cardiac hypertrophy, EMBO J. 25 (2006) 5305–5316. [PubMed: 17082763]

[20]. Rotter M, Sanders P, Takahashi Y, Hsu LF, Sacher F, Hocini M, Jais P, Haissaguerre M, Images in cardiovascular medicine. Coronary sinus tachycardia driving atrial fibrillation, Circulation 110 (2004) e59–60. [PubMed: 15302808]

[21]. Yamada T, Huizar JF, McElderry HT, Kay GN, Atrial tachycardia originating from the noncoronary aortic cusp and musculature connection with the atria: relevance for catheter ablation, Heart Rhythm 3 (2006) 1494–1496. [PubMed: 17161795]

[22]. Morita H, Zipes DP, Morita ST, Wu J, The role of coronary sinus musculature in the induction of atrial fibrillation, Heart Rhythm 9 (2012) 581–589. [PubMed: 22120133]

[23]. Sah R, Mesirca P, Mason X, Gibson W, Bates-Withers C, Van den Boogert M, Chaudhuri D, Pu WT, Mangoni ME, Clapham DE, Timing of myocardial trpm7 deletion during cardiogenesis variably disrupts adult ventricular function, conduction, and repolarization, Circulation 128 (2013) 101–114. [PubMed: 23734001]

[24]. Harada M, Luo X, Qi XY, Tadevosyan A, Maguy A, Ordog B, Ledoux J, Kato T, Naud P, Voigt N, Shi Y, Kamiya K, Murohara T, Kodama I, Tardif JC, Schotten U, Van Wagoner DR, Dobrev D, Nattel S, Transient receptor potential canonical-3 channel-dependent fibroblast regulation in atrial fibrillation, Circulation 126 (2012) 2051–2064. [PubMed: 22992321]

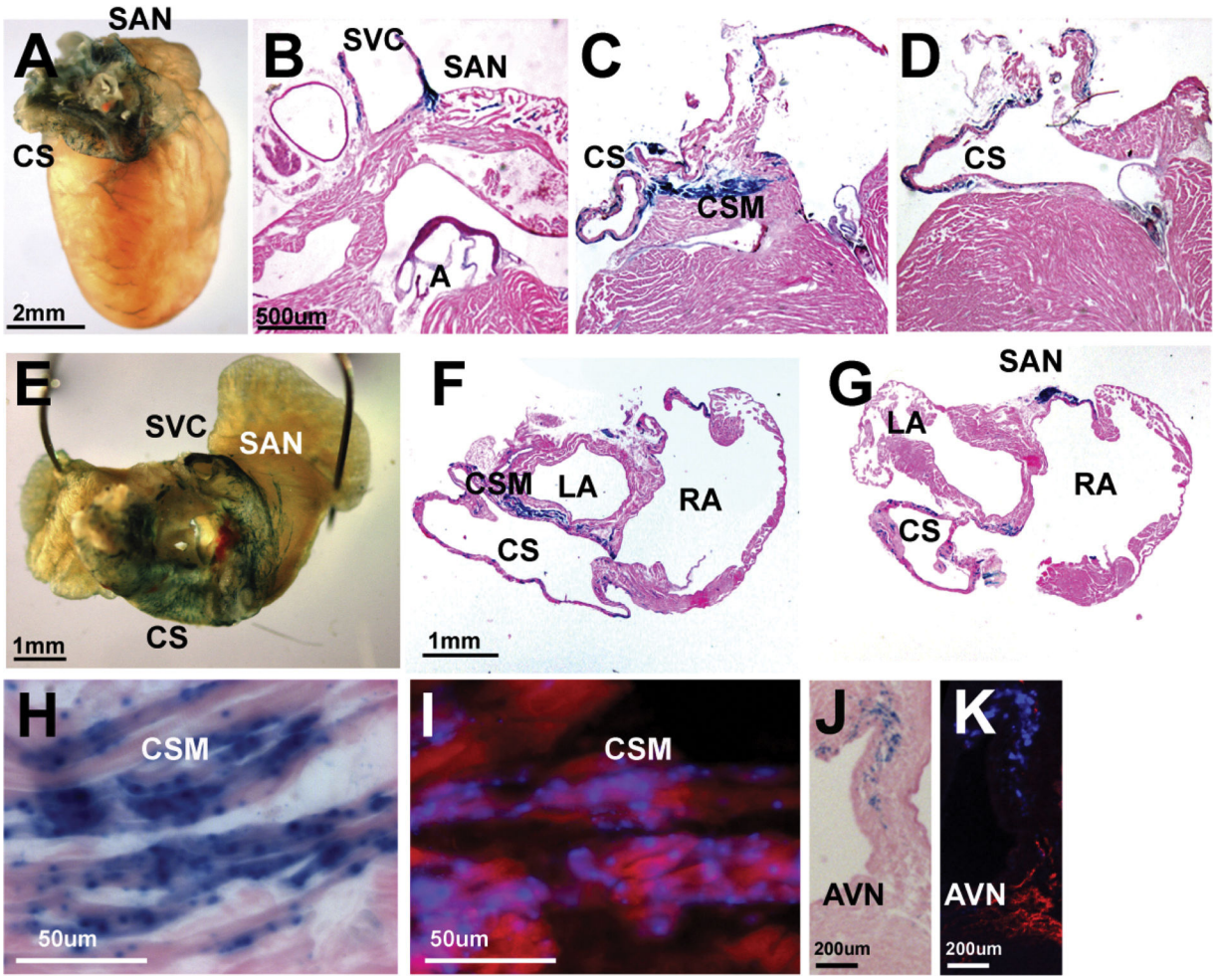

Fig. 1. Expression STIM1 in the interatrial conduction pathway from SAN to coronary sinus.

A. Posterior view of a whole mount STIM1-LacZ staining of a 3 week old $STIM1^{+/gt}$ mouse heart showing STIM1 expression in the SAN and coronary sinus. B–D. Sagittal wax sections of $STIM1^{+/gt}$ heart shown in A cut at 8 μm from paraffin and counter stained with Eosin. STIM1 was expressed in the SAN (B), musculature of coronary sinus (C) and coronary sinus (D). E. Whole mount LacZ staining of dissected atria and coronary sinus of an 8 week old $STIM1^{+/gt}$ heart. F–G. Cross sections of 8 week old $STIM1^{+/gt}$ heart (E), cut at 8 μm from paraffin and counter stained with Eosin. H–K High power images of frontal cryosections of P10 $STIM1^{+/gt}$ hearts cut at 14 μm. H. STIM1-LacZ (blue) in the cardiomyocytes of coronary sinus counterstained with Eosin I. Double labelling of STIM1-LacZ (inverted and colored blue) and MF-20 (red), a sarcomeric myosin marker. J. STIM1-LacZ (blue) in the atrial septum counterstained with Eosin. K. Double labelling of STIM1-LacZ (inverted and colored blue) and HCN4 a marker of the Atrioventricular node at p10. SAN- sinoatrial node, CS-coronary sinus, SVC- superior vena cava, CSM- coronary sinus musculature, LA-left atrium, RA-right atrium, A-aorta, AVN-Atrioventricular node.

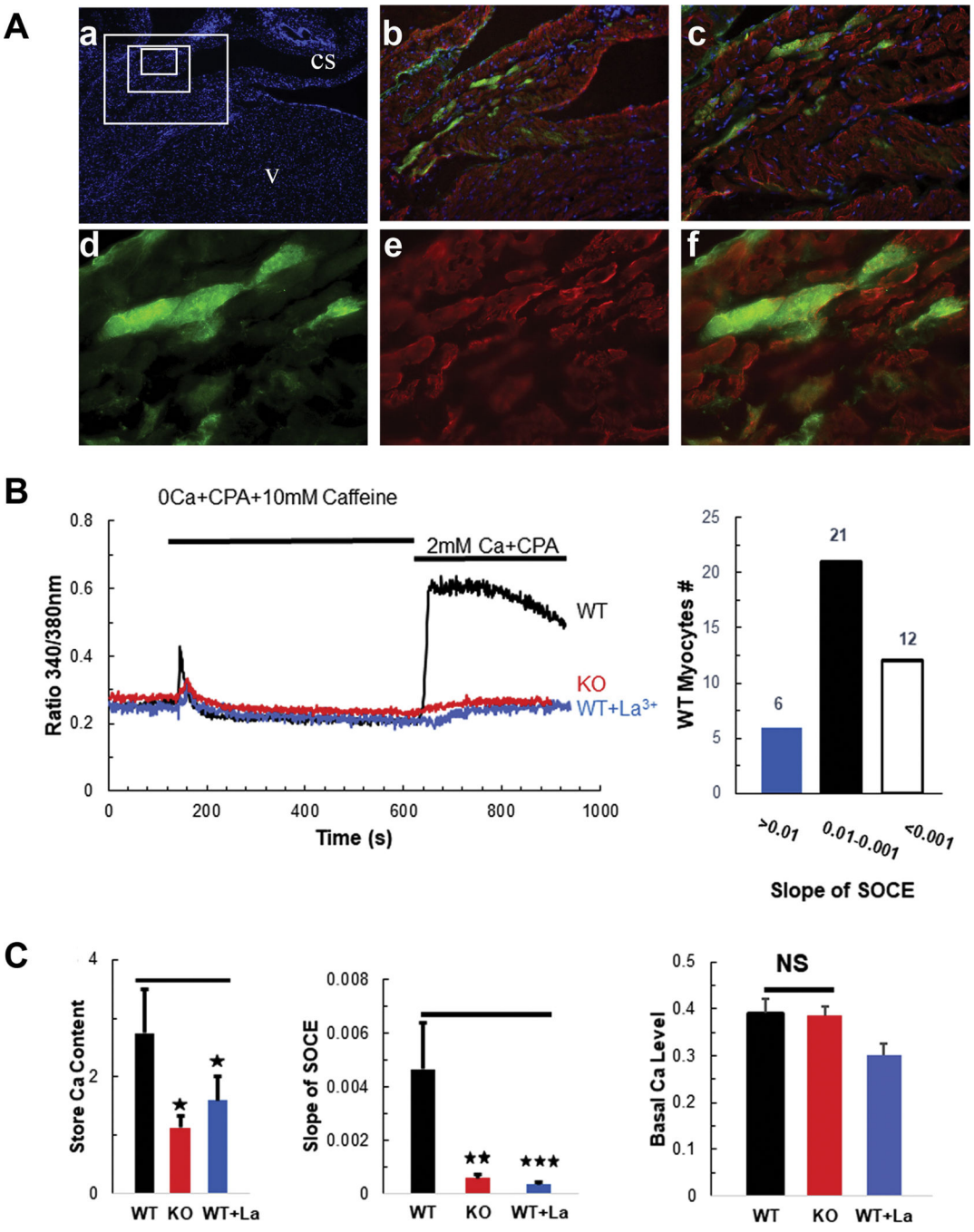

Fig. 2. Expression STIM1 in the interatrial conduction pathway from SAN to coronary sinus.

A. Immunofluoresence assessment of STIM1 in coronary sinus of the adult (16-weeks) mouse heart. Cryosection of the right atria were incubated with STIM1 and myosin heavy chain antibodies (MF20). DAPI staining provides architectural features to identify the coronary sinus (a). The square frames in A-a indicated where magnified images were showed in b–f. MF20+ cardiomyocytes are identified in the CS and STIM1 is expressed in a subset of CSC (b and c). A series of magnified images from the CS (a) reveal co-immunostaining for STIM1 and MF20 in WT hearts. B. Representative Fura-2 Ca^{2+}

measurements recorded from WT (black), KO (red) CSCs and a WT CS myocyte after treatment with 10 μM La^{3+} (blue). (left panel). Coronary sinus myocytes were counted and categorized by the extent of SOCE. A total of 39 CSCs were counted (Right panel). C. Summarized data of SR store Ca^{2+} content, slope of SOCE and basal Ca^{2+} (right panel). SR Ca^{2+} content (left panel) was determined as the area under the Ca^{2+} release curve following caffeine and CPA application, WT (n = 20), KO (n = 23) and WT + La^{3+} (n = 12) CS myocytes. In the middle panel showed summarized data of SOCE in the WT (n = 39), KO (n = 28) and WT + La (n = 15) CSCs. SOCE was markedly reduced in the KO CSCs and inhibited by 10 μM La^{3+}. Knock out of STIM1 in the CSCs did not alter basal cytosolic Ca^{2+} level.

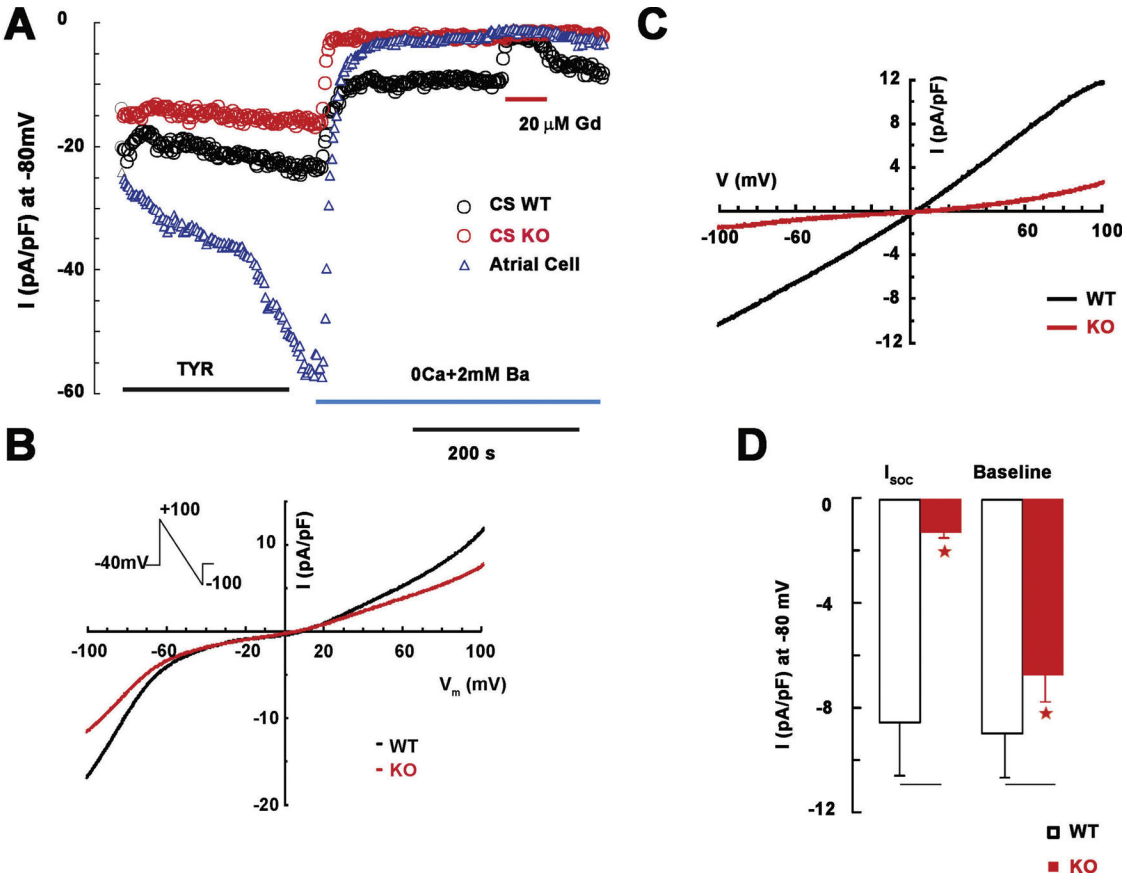

Fig. 3. Deletion of STIM1 from mouse heart markedly reduced I_{soc} and baseline current in CSCs.

A. Time course of current recordings at −80 mV from STIM1 WT (black circle), KO CSCs (red circle) and left atrial cells (blue triangle). B. Baseline currents recorded from WT (black, n = 10) and KO (red, n = 17) CSCs. Inset showed voltage protocol. C. IV curves for I_{soc} from WT (black, n = 10) and KO (red, n = 17) CSCs. I_{soc} was defined as 20 μM Gd^{3+} sensitive currents. D. Summarized data showed reduced I_{soc} and baseline currents at −80 mV in KO CSCs. Asterisk indicated the significance ($p < 0.05$).

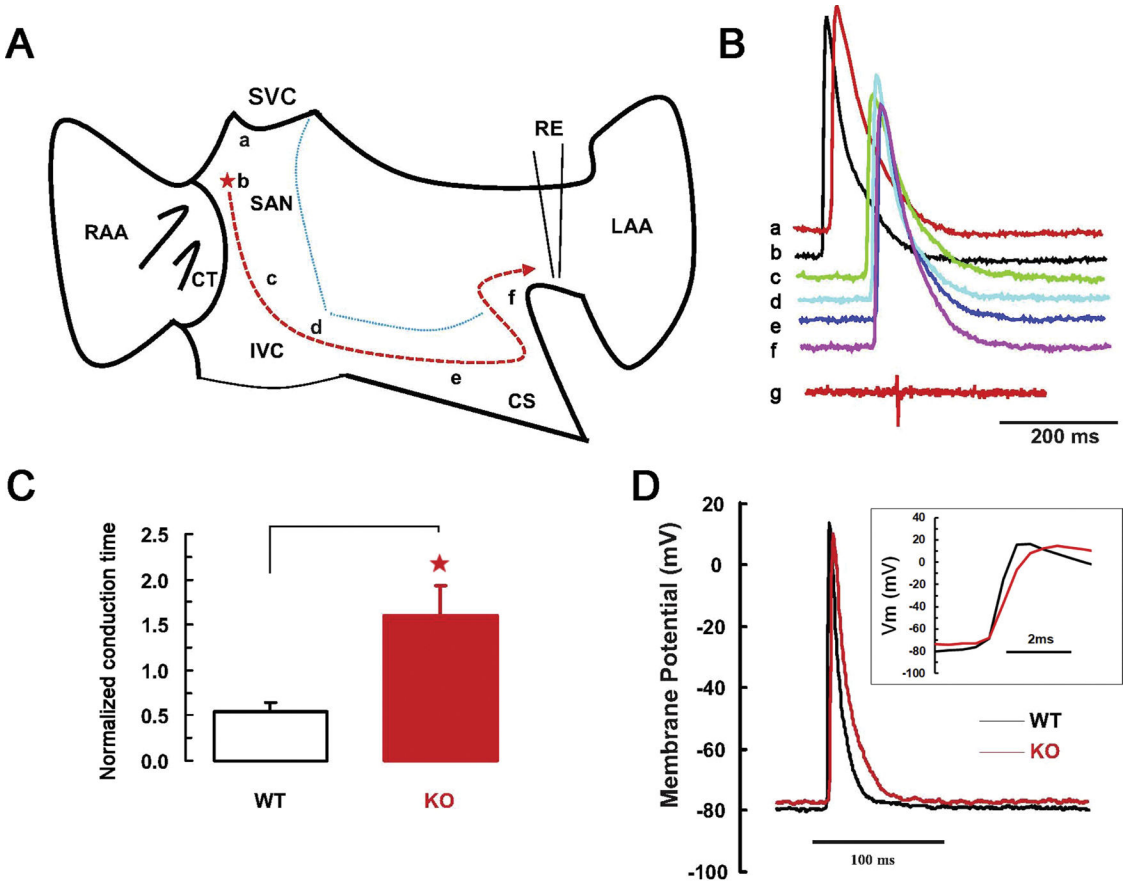

Fig. 4. Electrical mapping of pulses propagation from the SAN to left atria through coronary sinus in WT and KO mice.

A. Schematic view of interatrial conduction pathway through coronary sinus. Blue lines indicated where atrial septum and Bachmann's bundles were incised. a–f indicate where action potentials were recorded. B. Intracellular action potentials recorded in places as indicated in A from STIM1 WT mice. trace g was a surface potential recorded from left atria appendage. C. Changes in conduction time from SAN to left atria in the WT and KO mouse heart. D. Action potentials of CSCs from WT and KO mice. The inset showed a slow upstroke of action potential in the STIM1 KO CS. An asterisk indicated significance ($p < 0.05$).

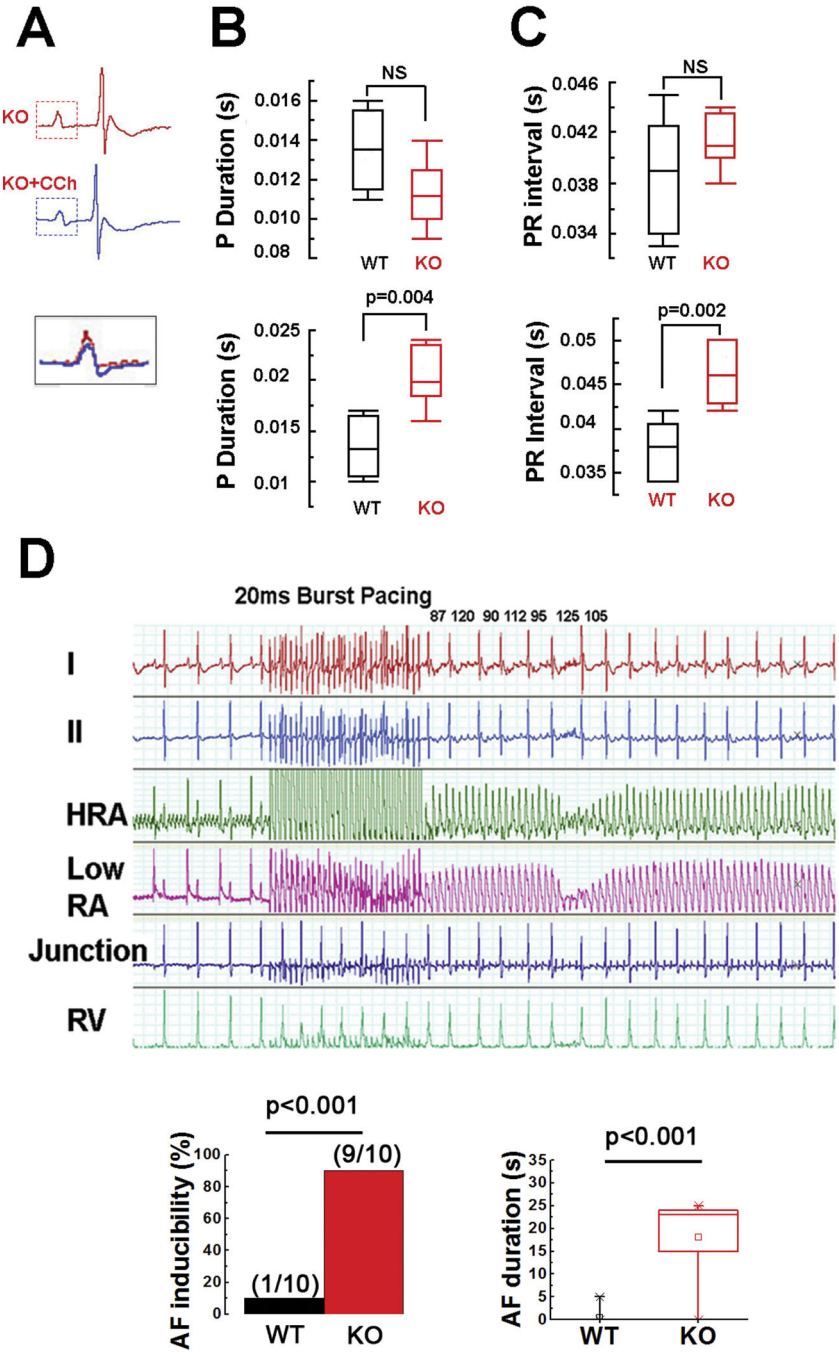

Fig. 5. Deletion of STIM1 from mouse heart changes P wave duration and triggers atrial arrhythmia.

A. Surface ECGs recorded from cSTIM1$^{-/-}$ mice with (blue trace, middle panel) or without (red trace, top panel) intraperitoneal injection of 100 ng/g CCh. Bottom panel showed superimposed P waves from cSTIM1$^{-/-}$ mice at baseline and with CCh, indicating that CCh induced a wider and biphasic P wave from cSTIM1$^{-/-}$ mice. B. no significant difference in P wave duration from STIM1$^{fl/fl}$ and cSTIM1$^{-/-}$ mice (top panel). P wave duration significantly increased in cStim1$^{-/-}$ mice (n = 5) with CCh compared to STIM1$^{fl/fl}$ mice (n = 5, bottom panel). C. No significant difference in PR interval from STIM1$^{fl/fl}$ and

cSTIM1$^{-/-}$ mice (top panel) at baseline. PR interval significantly increased in cStim1$^{-/-}$ mice (n = 5) with CCh compared to STIM1$^{fl/fl}$ mice (n = 5) (bottom panel). D. ECG and intracardiac potentials following rapid atrial pacing reveal induction of atrial fibrillation in cSTIM1$^{-/-}$ mice treated with CCh. A greater number of cSTIM1$^{-/-}$ mice were induced into AF compared to STIM1$^{fl/fl}$ mice (left). In addition the duration of AF was sustained for a greater period of time in the cSTIM1$^{-/-}$ mice (right).

Table 1

Action potential parameters of CSCs from WT and KO mice.

	WT	KO
RMP (mV)	−79.2 ± 2.0	−73.4 ± 1.8 *
APA (mV)	90.3 ± 5.8	80.6 ± 2.5
Overshoot (mV)	11.5 ± 5.1	7.4 ± 1.8
APD90 (ms)	31.8 ± 7.2	42.2 ± 2.6 *
Rate (mV/ms)	50.3 ± 11.0	± 2.8 *

* indicated the significance ($P < 0.05$, KO vs WT).